Automated quantitative microstructural analysis of metastatically involved vertebrae: Effects of stereologic model and spatial resolution

Hojjat S. P., and Whyne C. M.

Citation (published version) Hojjat SP, Whyne CM. Automated quantitative microstructural analysis of metastatically involved vertebrae: effects of stereologic model and spatial resolution. Med Eng Phys. 2011 Mar;33(2):188-94. doi: 10.1016/j.medengphy.2010.09.022. PMID: 21036094

Medical Engineering & Physics xxx (2010) xxx–xxx

Contents lists available at ScienceDirect

Medical Engineering & Physics

journal homepage: www.elsevier.com/locate/medengphy

Automated quantitative microstructural analysis of metastatically involved vertebrae: Effects of stereologic model and spatial resolution

Seyed-Parsa Hojjat[a,b], Cari M. Whyne[a,b,*]

[a] Orthopaedic Biomechanics Laboratory, Sunnybrook Health Sciences Centre, Room UB19, 2075 Bayview Avenue, Toronto, ON, Canada M4N 3M5
[b] Institute of Biomaterials & Biomedical Engineering Rosebrugh Building, University of Toronto, 164 College Street, Room 407, Toronto, ON, Canada M5S 3G9

ARTICLE INFO

Article history:
Received 17 April 2010
Received in revised form
27 September 2010
Accepted 30 September 2010

Keywords:
Spinal metastases
Automation
Bony architecture
Micro structure
Resolution

ABSTRACT

Summary of background data: Preclinical models of spinal metastases allow for the application of micro-image based structural assessments, however, large data sets resulting from high resolution scanning motivates a need for robust automated analysis tools. Accurate assessment of changes in vertebral architecture, however, may depend both on the resolution of images acquired and the models used to represent the structural data.

Objective: To apply a recently developed automated μCT based analysis tool to quantify the effect of diffuse metastatic disease on rat vertebral architecture at multiple resolutions. It was hypothesized that automated methods could accurately quantify differences in vertebral microstructure and that diffuse metastatic disease could be shown to have significant negative architectural effects on trabecular bone independent of stereologic model and resolution.

Methods: μCT images acquired at 14 μm^3 of healthy and metastatcially involved whole lumbar rat vertebrae were analyzed at high, medium and low (8.725, 17.45, and 34.9 μm^3) resolutions using an automated algorithm to yield micro-structural measures of the trabecular centrum and cortical shell. The images analyzed at different resolutions were obtained via up/downsampling of the acquired image data. Trabecular thickness was evaluated with the Parfitt and Hildebrand models, and anisotropy evaluated through mean intercept length.

Results: Significant differences in microstructural parameters measured in comparing healthy and metastatically involved vertebrae were affected by resolution, however, relative anisotropy was maintained. The Parfitt and Hilderbrand models yielded similar structural differences between healthy and metastatic vertebrae, however, the Hildebrand model was limited due to segmentation accuracy required for its automated application.

Conclusions: Differences in microstructural parameters generated through automated analysis at high resolution suggest that diffuse MT1 osteolytic destruction in whole rat vertebrae results primarily in loss of trabeculae in the metastatic vertebrae, as opposed to trabecular thinning. The sensitivity of the bony architectural parameters to resolution motivates the need for high resolution scanning or post-processing of images.

1. Introduction

Metastatic spread of cancer to the skeleton most frequently affects the spinal column. Vertebral metastases can result in skeletal related events (SREs) such as extreme pain, pathologic fracture and neurologic compromise, and cause a significant decline in patients' quality of life [1–5]. Clinically, accurate prognoses for spinal metastases remain a challenge [6]. This, in part, may be due to the qualitative or semi quantitative nature of currently available assessment schemes. The lack of quantitative measures for evaluation of disease in patients with spinal metastases results in difficulties related to clinical decision-making and the exclusion of these patients from many clinical trials. Considering the high occurrence of spinal metastases, there is a need for a robust quantitative method to evaluate the structural burden of spinal metastases.

Preclinical models are widely used to study spinal metastases [7]. Preclinical skeletal lesions are most commonly developed through either local or intracardiac injection of cancer cell lines. The evaluation of resultant metastatic tumor burden in bone and its effect on the skeletal microstructure has also mainly been qualitative or semi quantitative [7,8]. In semi quantitative analyses, it is

* Corresponding author at: Orthopaedic Biomechanics Laboratory, Sunnybrook Health Sciences Centre, Room UB19, 2075 Bayview Avenue, Toronto, ON, Canada M4N 3M5. Tel.: +1 416 480 5056; fax: +1 416 480 5856.
E-mail addresses: parsa.hojjat@utoronto.ca (S.-P. Hojjat), cari.whyne@sunnybrook.ca (C.M. Whyne).

1350-4533/$ – see front matter © 2010 IPEM. Published by Elsevier Ltd. All rights reserved.
doi:10.1016/j.medengphy.2010.09.022

common to quantify bone quality using manually selected regions of interest (ROI). This approach, however, can limit the repeatability of measurements through the introduction of inter and intraobserver errors and potential bias. These errors may be caused by the manual omission of regions that may not be visually affected by the tumor but may contribute to the mechanical integrity of the structure.

Bone quality is often assessed via architectural models that are correlated with mechanical stability. The plate model developed by Parfitt et al. [9] has long been used to describe the architecture of trabecular bone [10–18]. The Parfitt plate model calculates trabecular thickness, spacing and number through formulae derived based on bone volume and surface area. The Parfitt plate model makes the assumption that all trabeculae are plates, which is a limitation particularly in the consideration of low density trabecular bone or bone compromised by pathology such as osteolytic disease. More recently, Hilderbrand and ~~Ruegsegger~~ [19] proposed a new method for characterizing the architecture of trabecular bone that calculates trabecular thickness without any structural assumptions. The Hilderbrand method defines trabecular thickness at every point as the diameter of the biggest sphere that could perfectly fit inside the trabeculae. Using histograms, they demonstrated a range of trabecular thickness values within human bone samples, and a trabecular structure composed of both plates and rods. This work concluded that the Parfitt model over estimates trabecular thickness due to the plate assumption.

Mechanical structure can further be evaluated based on the degree of anisotropy in a material. Bone has been shown to have transversely isotropic material properties, with the degree of anisotropy related to bone density. The mean intercept length (MIL) method has been utilized to estimate the degree of anisotropy within trabecular bone structures [20]. MIL is defined as the average distance between the intercepts made by a line in a specific direction with the mesh of interest (i.e. trabecular mesh). The MIL for an isotropic object is the same for any line intercepting the mesh in any direction.

High resolution μCT is often used for visualization of trabecular structure in preclinical models. Depending on the size of the sample and the image resolution, a μCT scan can occupy as much as 10 GB of ~~memory~~. Accurate quantitative analysis of such large image data files can be time consuming requiring a robust automated analysis tool for widespread utilization. One method of compensation is to downsample images before processing. However, downsampling can cause blurring effects in images and result in changes in measured microstructural parameters [21,22]. An automated quantitative analysis tool that is robust enough to function at a variety of resolutions can be utilized to determine the importance of resolution in characterizing and tracking pathological changes in bony structures. Such a tool would further facilitate analysis in preclinical studies of skeletal metastatic disease to yield accurate and precise quantification of the effects of new and existing treatments on bony architecture.

Qualitative analysis shows the apparent destruction of trabecular structure in the presence of large skeletal metastases. However, characterization of less severe more diffuse patterns of metastatic disease is more challenging. The objective of this work was to apply a recently developed automated μCT based analysis tool to quantify the effect of diffuse metastatic disease on the architecture of the rat spine at multiple resolutions. It was hypothesized that automated methods can be used to accurately quantify the microstructural effects of metastatic disease in the rat spine and that diffuse metastatic disease can be shown to have significant negative architectural effects on trabecular bone using either the Parfitt or the Hilderbrand model at different resolutions.

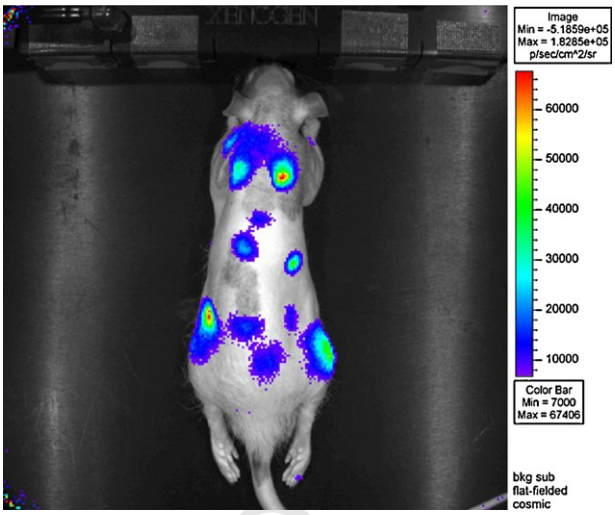

Fig. 1. Intracardiac injection of luciferase transfected human carcinoma cells yielded distinct vertebral metastases 2–3 weeks after cell inoculation into rnu/rnu rats as demonstrated by bioluminescent imaging.

2. Materials and methods

2.1. Model development

Lumbar vertebrae from healthy ($n = 6$) and metastatic ($n = 6$) rats were utilized for the study. Osteolytic spinal metastases were developed through intracardiac injection of human MT1 breast cancer cells into 4-week-old rnu/rnu rats. The MT1 cell line had previously been transfected with the luciferase gene to enable identification of tumor within the vertebrae using bioluminescent imaging. Lumbar vertebrae (L1, L2 or L3) with metastatic tumor were identified 21 days after cell inoculation with bioluminescent imaging prior to sacrifice (Fig. 1, IVIS Bioluminescent Imaging System).

2.2. Image acquisition

Following sacrifice, the rat spines were excised and imaged using a high resolution digital μCT scanner (14 μm^3 resolution, GE Explore Locus, General Electric Company, Fairfield, USA). μCT imaging of whole vertebrae yields 3D high resolution images of the high intensity cortical and trabecular bone tissue, with bone marrow and lytic tumor appearing as low intensity values which were not distinguishable from each other.

2.3. Automated segmentation

A previously designed automated segmentation algorithm was used to segment the whole vertebrae, the trabecular centrum and the individual trabecular structure [24]. The whole vertebral images were manually aligned to a global axis prior to the automated segmentation algorithm to ensure convergence (AmiraDev) [25]. The remainder of the process was carried out in a fully automated fashion. The segmentation algorithm began with an affine registration to register a manually segmented atlas to the vertebra of interest. This was followed by a multi-resolution demons deformable registration of the atlas to the target vertebra to ensure accurate segmentation. Level set filtering was then used to refine the demons segmentation to yield a smooth segmentation curve, accurately outlining the boundaries of the whole vertebra in spite of the discontinuities present in the shell due to metastatic destruction as well as the nerves and vessels entering the vertebral body. The whole vertebral segmentation boundaries were then contracted

Please cite this article in press as: Hojjat S-P, Whyne CM. Automated quantitative microstructural analysis of metastatically involved vertebrae: Effects of stereologic model and spatial resolution. Med Eng Phys (2010), doi:10.1016/j.medengphy.2010.09.022

while maintaining the curvature to segment the trabecular centrum. This was done using another multi-iteration application of the level set filter. Once the trabecular centrum was segmented, edge-preserving upsampling followed by intensity-based thresholding were utilized to segment the individual trabecular structure (Fig. 2).

2.4. Morphological measurements

Stereologic analysis was automated within the AmiraDev 5 [25] platform to yield measures of: total vertebral volume (TVV), total volume of the trabecular centrum (TV), bone volume in the trabecular centrum (BV), trabecular bone surface area (BS), as well as the degree of anisotropy using the mean intercept length (MIL) method. Cortical bone volume (CBV) was calculated as the volume of the whole vertebrae (TVV) minus the total volume of the trabecular centrum (TV). The Parfitt plate model was employed to calculate parameters representing trabecular bone volume (TBV), trabecular thickness (TbTh), trabecular number (TbN) and trabecular spacing (TbS) as per Eq. (1)

$$\begin{aligned} \mathrm{TBV} &= \mathrm{BV}/\mathrm{TV} \\ \mathrm{TbTh} &= \frac{2}{\mathrm{BS}/\mathrm{BV}} \\ \mathrm{TbN} &= \frac{\mathrm{TBV}}{\mathrm{TbTh}} \\ \mathrm{TbS} &= \frac{1}{\mathrm{TbN}} - \mathrm{TbTh} \end{aligned} \tag{1}$$

Trabecular thickness was additionally calculated using the Hilderbrand model. In this model, trabecular local thickness at every point is calculated as the diameter of the largest sphere that can perfectly fit inside the trabecula without crossing its borders [19]. To implement this model we calculated the 3D float Chamfer map at every point of the generated individual trabecular segmentation to calculate the closest distance at every point from the background. The Chamfer map is a close approximation of the Euclidean distance map and is the preferred choice for larger datasets due to its efficiency [23]. Chamfer maps are widely used in skeletonization applications (AmiraDev) [25]. The 3D center line of the distance map represents the radius of the biggest sphere that perfectly fits in each trabecula at every point. Doubling the radius value yields the local trabecular thickness at each point (i.e. the diameter of the largest sphere that could perfectly fit into the trabecula). To implement this, we constructed a 3D skeleton from the trabecular segmentation (Amira 5 Skeletonization Pack) [25] and performed an element wise multiplication with the double of the distance map matrix. The automated algorithm was validated using structures of known thickness (Fig. 3). The first and simplest test structure was a cylinder of a known thickness. The second structure was composed of four parallel cylinders of the same thickness intersected by plates of the same width. The significance of the second figure was to test the ability of the algorithm to skeletonize organized connected structures of uniform thickness. The final test structure was meant to mimic the trabecular structure as it was composed of struts of variable thickness and orientation. We validated the accuracy of the algorithm by evaluating its ability to skeletonize, and yield the correct thickness histogram.

Mean intercept length (MIL) was calculated in the superoinferior (X), mediolateral (Y) and dorso-frontal (Z) directions [20]. The MIL was automatically calculated by shifting the binary image of the individual trabecular segmentation by 1 voxel in the direction of interest and subtracting the result from the original image. The number of non-zero voxels in the resulting image were counted and divided by two to yield the number of intercepts in the direction of interest. The total length in the direction of interest was calculated

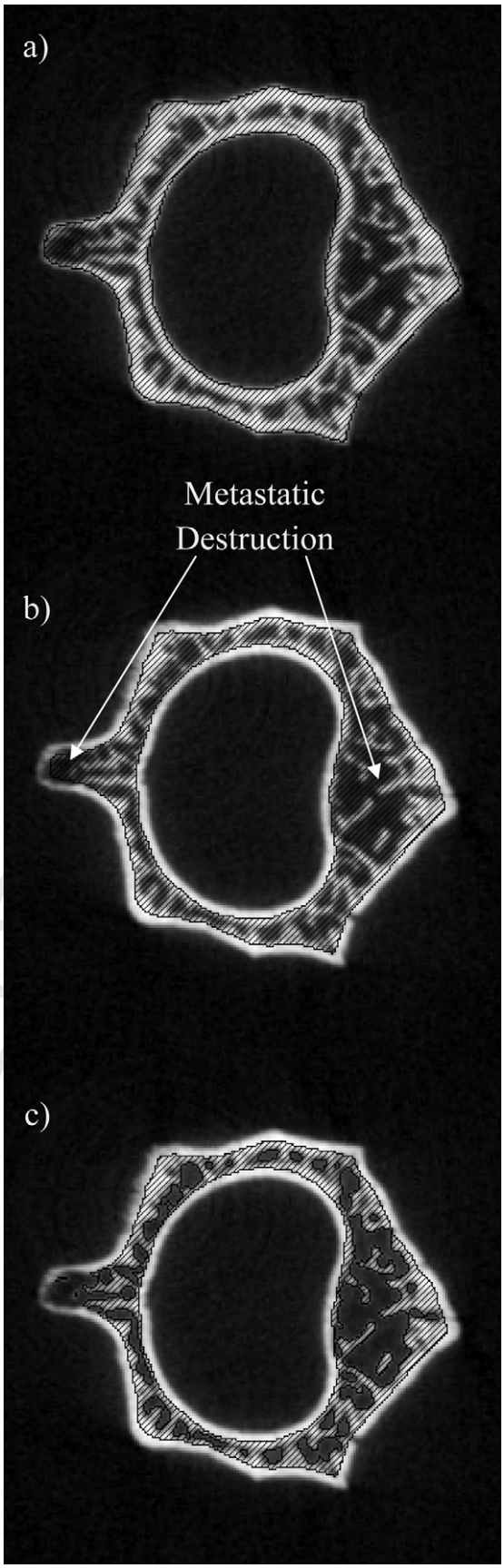

Fig. 2. Axial slice outputs at each stage of the program: (a) segmentation of the whole vertebrae, (b) removal of the cortical shell, and (c) individual trabecular segmentation.

Please cite this article in press as: Hojjat S-P, Whyne CM. Automated quantitative microstructural analysis of metastatically involved vertebrae: Effects of stereologic model and spatial resolution. Med Eng Phys (2010), doi:10.1016/j.medengphy.2010.09.022

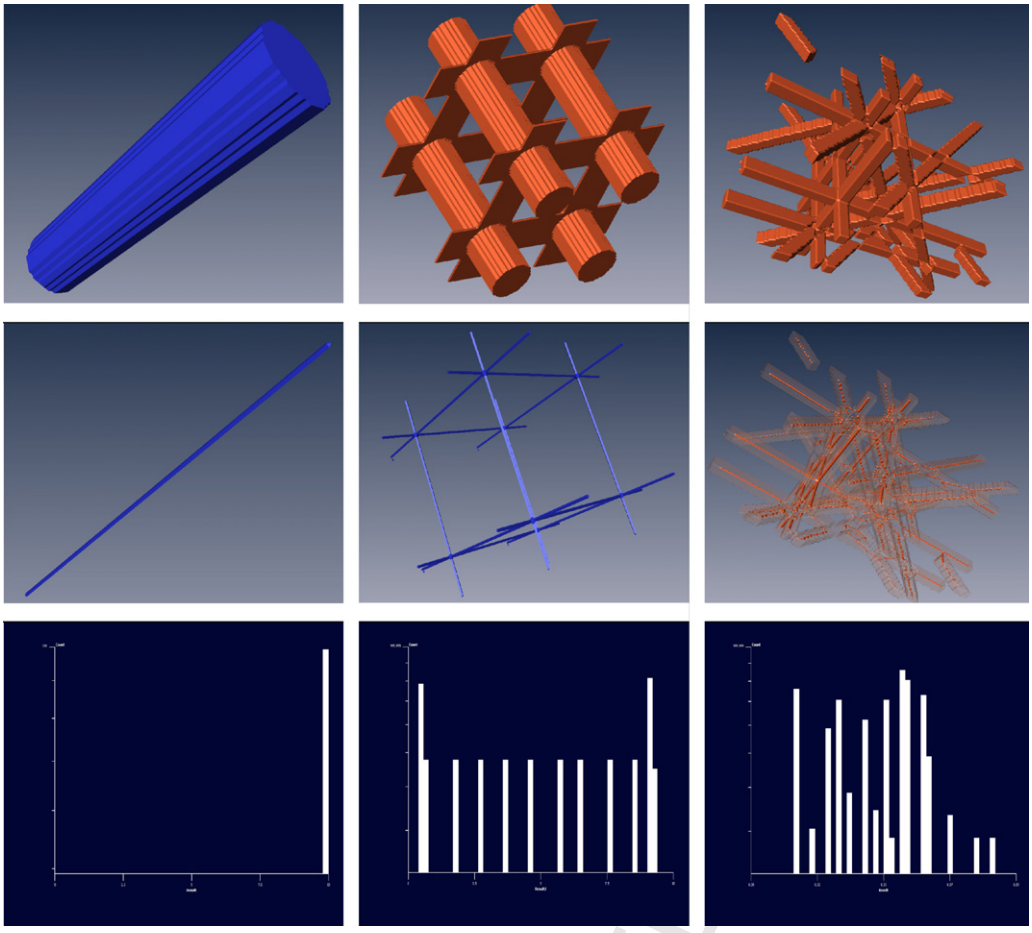

Fig. 3. Designed test structures of constant and variable thickness and orientation (top row), the extracted center lines (middle row), and thickness histograms (bottom row).

as the total volume divided by the average cross sectional area of the perpendicular plane. Dividing the total length by the total number of intercepts yielded the MIL measure in each direction of interest [Eq. (2)].

$$\widetilde{A} = T(A)$$
$$I\varphi = \frac{numel(\widetilde{A} \neq A)}{2}$$
$$L\varphi = \frac{V}{CSA} \quad (2)$$
$$\mathrm{MIL}\varphi = \frac{L\varphi}{I\varphi}$$

In the above equation set T represents the transformation performed on the binary image (A) to yield the transformed image ($\widetilde{A}$). $I\varphi$ and $L\varphi$ represents the number of intercepts and the length in the orientation of interest (φ), respectively. Finally MILφ corresponds to the mean intercept length in the orientation φ.

The MIL values for an isotropic structure remain consistent in all directions. This automated approach quantifies the degree of anisotropy of the structure in a less general manner in comparison to the original work presented by Odgaard [20] as it only calculates the MIL in three orientations.

2.5. Resolution

All of the parameters described above were calculated at 8.725 μm × 8.725 μm × 8.725 μm (high), 17.45 μm × 17.45 μm × 17.45 μm (medium), and 34.9 μm × 34.9 μm × 34.9 μm (low) isotropic spatial resolutions. The data at different resolutions were obtained by resampling the image data which were acquired at 14 μm × 14 μm × 14 μm.

2.6. Statistical analysis

Normality of the distribution of the structural measures was verified using one sample Kolmogorov–Smirnov (KS) test (SPSS statistical software) [26]. Two tailed t-tests were then used to

Table 1
Micro-structural measures of the healthy and metastatic vertebrae at high (8.725 μm^3), medium (17.5 μm^3) and low (34.9 μm^3) resolution.

Attribute	Healthy (n = 6)			Metastatic (n = 6)		
	8.725 μm^3	17.5 μm^3	34.9 μm^3	8.725 μm^3	17.5 μm^3	34.9 μm^3
TBV (%)	55.92 ± 3.2	56.12 ± 3.4	55.77 ± 3.3	50.37 ± 2.5	50.35 ± 2.3	50.78 ± 2.3
TbN (#/mm^2)	5.70 ± 0.77	3.04 ± 0.11	1.91 ± 0.07	4.58 ± 0.19	3.44 ± 0.07	2.16 ± 0.09
TbS (μm)	78 ± 13	144 ± 11	232 ± 22	109 ± 6	144 ± 8.7	228 ± 19
Parfitt's TbTh (μm)	100 ± 17	184 ± 14	292 ± 16	110 ± 8	147 ± 7	234 ± 8
Hilderbrand's TbTh (μm)	87 ± 21	104 ± 25	203 ± 13	100 ± 13	116 ± 9	132 ± 13
CBV (cm^3)	0.0411 ± 0.006	0.0412 ± 0.006	0.0409 ± 0.006	0.0293 ± 0.007	0.0295 ± 0.007	0.0290 ± 0.007

Please cite this article in press as: Hojjat S-P, Whyne CM. Automated quantitative microstructural analysis of metastatically involved vertebrae: Effects of stereologic model and spatial resolution. Med Eng Phys (2010), doi:10.1016/j.medengphy.2010.09.022

Table 2
Mean intercept length (μm) of the healthy and metastatically involved vertebrae measured high (8.725 μm^3, ~~shaded~~), medium (17.5 μm^3) and low (34.9 μm^3) resolution.

Direction	Healthy			Metastatic		
	8.725 μm^3	17.45 μm^3	34.9 μm^3	8.725 μm^3	17.45 μm^3	34.9 μm^3
X	66 ± 14	64 ± 12	76 ± 14	88 ± 26	97 ± 10	105 ± 15
Y	67 ± 12	66 ± 10	79 ± 12	92 ± 28	100 ± 10	108 ± 13
Z	96 ± 19	89 ± 18	111 ± 20	133 ± 39	145 ± 20	157 ± 26

compare the structural measures generated from the healthy and metastatically involved vertebrae. Similar analyses were applied to compare thickness values obtained using Parfitt's plate model with the values measured using Hilderbrand's model, assuming unequal variances.

3. Results

Diffuse osteolytic vertebral metastases secondary to MT1 injection were confirmed through bioluminescent imaging in 6 lumbar vertebrae (2 L1, 3 L2 and 1 L3 vertebrae) generated from 4 rats. A similar cohort of vertebrae (2 L1, 3 L2 and 1 L3 vertebrae) were analyzed from 6 healthy rats.

3.1. Parfitt plate model

Using the output of the automated segmentation algorithm, the Parfitt plate model showed a significant decrease in TBV, TbN and CBV and a significant increase in TbS in the metastatic vertebrae in comparison to the healthy group at the highest resolution ($p < 0.05$). There was no significant difference in TbTh (Parfitt model, $p = 0.22$; Hilderbrand model, $p = 0.20$) between the healthy and metastatic groups at the highest resolution (Table 1).

3.2. Hilderbrand model

The automated thickness calculation method using Hilderbrand model yielded accurate results when applied to objects of known thickness. Fully automated calculation of trabecular thickness based on the generated individual trabecular segmentation using the algorithm proposed by Hilderbrand et al. was limited due to the presence of a low number of small islands created in the thresholding stage of the automated segmentation. As the Hilderbrand model assigns a thickness to every structure segmented as bone, presence of the islands of negligible thickness drastically reduces the average trabecular thickness measured.

Time consuming manual island removal was required to ensure appropriate removal of islands without removing any of the trabecular bone structure. Once the islands were manually removed, similar results to the Parfitt model were found demonstrating no significant change in trabcular thickness in comparing the healthy and metastatically involved vertebrae at the highest resolution (Table 1). While the average trabecular thickness measures were lower using the Hilderbrand model as compared to the Parfitt model for both the healthy and the metastatically involved vertebrae, this result was not significant ($p = 0.09$ for high, 0.09 for medium, and 0.2 for low resolution levels).

3.3. Mean intercept length (MIL)

Transverse isotropy of the trabecular structure was found in both the healthy and the metastatic vertebrae, demonstrating significantly higher MIL values in the axial (*Z*) direction as compared to the transverse (*X* and *Y*) directions. As expected, the MIL values were found to be higher in the metastatic group in all directions due to tumor destruction; however, no difference in the relative degree of anisotropy was observed as the ratio of MIL values in the axial direction to the values in the transverse directions remained consistent (~1.5:1) (Table 2).

3.4. Resolution

All of the micro-structural parameters in the healthy and metastatically involved vertebrae were measured at 17.45 μm × 17.45 μm × 17.45 μm and 34.9 μm × 34.9 μm × 34.9 μm isotropic resolution levels and compared to the highest resolution (8.725 μm × 8.725 μm × 8.725 μm) results. TBV at all resolutions was higher in the healthy group. TbTh values were significantly affected by resolution. In comparison to the lack of a difference measured at the highest resolution, larger TbTh values were calculated in the healthy vs. the metastatic group at both the medium and the low resolutions for both the Parfitt and the Hilderbrand models. TbN decreased significantly as the resolution was lowered. In direct contrast to the highest resolution, TbN values were found to be significantly larger in metastatically involved vertebrae at medium and low resolutions. TbS increased significantly as the resolution was lowered and, again in contrast to findings at the highest resolution, no significant differences were found in TbS values at medium and low resolutions (Table 1). At all resolutions, MIL values remained consistent, with lower values but similar amounts of anisotropy in comparing the healthy and metastatically involved vertebrae (Table 2).

4. Discussion

This work demonstrates the ability of an automated algorithm to quantify microstructural differences in healthy vertebrae vs. vertebrae with diffuse osteolytic metastatic disease based on μCT image data at multiple resolutions. The accurate automated method enables objective and repeatable analysis of multiple morphologic measures and allows the comparison of two distinct models for describing trabecular thickness (Parfitt and Hilderbrand).

The automated segmentation method used in this study has been previously validated against manual segmented data [24]. Excellent volumetric concurrency was demonstrated between the automated and manual segmentation techniques for whole vertebrae, trabecular centrums and individual trabecular networks (95–98%).

The morphologic measurements generated using the automated algorithm demonstrated expected significant differences between microstructural bone measures in comparing the healthy and metastatic vertebrae. Significant decreases in CBV, TBV, TbN and a significant increase in TbS were observed in the metastatic group when compared to the healthy group at the highest resolution. Both the widely used Parfitt plate model and the Hilderbrand model demonstrated no significant difference in TbTh between the two groups at the highest resolution. This supports the idea that the osteolytic destruction results primarily in loss of trabeculae as opposed to trabecular thinning [16].

The Hilderbrand model required further manual refinement of the automated segmentation to yield correct results. This was due to the presence of limited number of isolated islands, which were assigned an extremely low thickness value resulting in a considerable drop in the average trabecular thickness. The Parfitt plate

Please cite this article in press as: Hojjat S-P, Whyne CM. Automated quantitative microstructural analysis of metastatically involved vertebrae: Effects of stereologic model and spatial resolution. Med Eng Phys (2010), doi:10.1016/j.medengphy.2010.09.022

We have confirmed this finding, demonstrating an increase in measured trabecular thickness, using both the Parfitt and the Hilderbrand models, as resolution is reduced. Structural differences in comparing normal vertebrae to those with diffuse metasatic involvement were affected by resolution. However, as the severity of the metastatic involvement increases, significant structural differences may be more consistently identified at lower resolutions.

Other works have looked at determining an optimum resolution for imaging trabecular bone for different applications [28,29]. Peyrin et al. [28] acquired μCT images from human vertebrae at 2, 7, and 14 μm isotropic voxel size and noted that 14 μm provided sufficient structural detail. This was however, concluded via qualitative observation. Muller et al. [22] in studying the effects of resolution on quantification of the microstructure of the human iliac crest also concluded that isotropic resolution of 14 μm yielded correct values for the microstructural parameters. They noted that microstructural parameters increase or decrease monotonously as a function of resolution, and thus commented that a suitable calibration procedure could be used to restore the correct data. We also observed this monotonous behavior in the microstructural parameters analyzed at different resolutions in our data. Niebur et al. performed a convergence study to determine the optimal resolution for micro finite element modeling and have concluded that the optimum acquisition resolution should be about 1/4 of average trabecular thickness [29]. Resolution studies in preclinical models are more limited, however. Bouxsein et al. [30] have performed a comprehensive study on μCT based assessment of microstructure in rodents. While the minimum ratio of voxels to object size is reported as 2, the authors noted that this ratio should ideally be higher (3–4 voxels) for accurate morphologic measurements and finite element model generation. The trabecular dimensions in rat vertebrae have been described to be in the range of 60 μm, similar to the findings at the highest resolution for the healthy rat vertebrae in this study (87 ± 21 μm). As such, utilization of an isotropic voxel size of 14 μm during image acquisition is acceptable based on the 3–4 voxel per trabecula guideline. However, we found that further upsampling of the acquired data to obtain a sharper image enabled us to more smoothly segment the trabecular structure.

Robust automated microstructural analyses can be used to facilitate accurate evaluation of the effects of new and existing treatments aimed at spinal lesions in preclinical models. Overall the presented work suggests that automated use of Parfitt's plate model along with the MIL method can be used to yield quantitative analyses demonstrating differences in vertebral microstructure due to moderate metastatic involvement. However, the sensitivity of many of the architectural parameters to resolution motivates the need for high resolution scanning or post-processing of images to reduce blurring in future preclinical applications.

Acknowledgments

This work was supported by Canadian Institute of Health Research (CIHR) Grant # 724180902.

The authors would like to thank Dr. Margarete Akens for her work on the preclinical model, and Dr. Maarten Beek for his computational assistance.

Conflict of interest statement

The authors do not have any conflict of interest.

References

[1] Wong DA, Fornasier VL, McNab I. Spinal metastases: the obvious, the occult, and the imposters. Spine 1990;15(1):1–3.
[2] Houston, Rubens RD. The systemic treatment of bone metastases. Clinical Orthopaedics and Related Research 1995;312:95–104.
[3] Toma, Venturino A, Sogno G, et al. Metastatic bone tumors. Nonsurgical treatment. Outcome and survival. Clinical Orthopaedics and Related Research 1993;295:246–51.
[4] Coleman R, Rubens R. The clinical course of bone metastases from breast cancer. British Journal of Cancer 1987;55:61–6.
[5] Hill ME, Richards MA, Gregory WM, Smith P, Reubens RD. Spinal cord compression in breast cancer: a review of 70 cases. British Journal of Cancer 1993;68(5):969–73.
[6] Leithner A, Radl R, Gruber G, et al. Predictive value of seven preoperative prognostic scoring systems for spinal metastases. European Spine Journal 2008;17:1488–95.
[7] Burch S, Bisland S, Wilson B, et al. Multimodality imaging strategies for vertebral metastases in a preclinical osteolytic model. Clinical Orthopaedics and Related Research 2007;454:230–6.
[8] Burch S, Bisland SK, Bogaards A, et al. Photodynamic therapy for the treatment of spinal metastases. Journal of Orthopaedic Research 2005;23(September (5)):995–1003.
[9] Parfitt AM, Mathews CH, Villanueva AR, et al. Relationships between surface, volume, and thickness of iliac trabecular bone in aging and in osteoporosis. Implications for the microanatomic and cellular mechanisms of bone loss. Journal of Clinical Investigation 1983;72(October (4)):1396–409.
[10] Agarwal SC, Dumitriu M, Tomlinson GA, et al. Medieval trabecular bone architecture: the influence of age, sex, and lifestyle. American Journal of Physical Anthropology 2004;124(May (1)):33–44.
[11] Banse X, Devogelaer JP, Grynpas M. Patient-specific microarchitecture of vertebral cancellous bone: a peripheral quantitative computed tomographic and histological study. Bone 2002;30(June (6)):829–35.
[12] Banse X, Devogelaer JP, Munting E, et al. Inhomogeneity of human vertebral cancellous bone: systematic density and structure patterns inside the vertebral body. Bone 2001;28(May (5)):563–71.
[13] Benhamou CL. Effects of osteoporosis medications on bone quality. Joint Bone Spine 2007;74(January (1)):39–47. Epub 2006 November 28.
[14] Ito M, Nishida A, Koga A, et al. Contribution of trabecular and cortical components to the mechanical properties of bone and their regulating parameters. Bone 2002;31(September (3)):351–8.
[15] Kinney JH, Haupt DL, Balooch M, et al. Three-dimensional morphometry of the L6 vertebra in the ovariectomized rat model of osteoporosis: biomechanical implications. Journal of Bone and Mineral Research 2000;15(October (10)):1981–91.
[16] Kurth AA, Müller R. The effect of an osteolytic tumor on the three-dimensional trabecular bone morphology in an animal model. Skeletal Radiology 2001;30(February (2)):94–8.
[17] Lane NE, Yao W, Kinney JH, et al. Both hPTH(1–34) and bFGF increase trabecular bone mass in osteopenic rats but they have different effects on trabecular bone architecture. Journal of Bone and Mineral Research 2003;18(December (12)):2105–15.
[18] Sone T, Tamada T, Jo Y, Miyoshi H, Fukunaga M. Analysis of three-dimensional microarchitecture and degree of mineralization in bone metastases from prostate cancer using synchrotron microcomputed tomography. Bone 2004;35(August (2)):432–8.
[19] Hilderbrand T, Ruegsegger P. A new method for the model-independent assessment of thickness in three-dimensional images. Journal of Microscopy 1997;185:67–75.
[20] Odgaard A. Three-dimensional methods for quantification of cancellous bone architecture. Bone 1997;20(April (4)):315–28.
[21] Hangartner TN. Thresholding technique for accurate analysis of density and geometry in QCT, pQCT and μCT images. Journal of Musculoskeletal and Neuronal Interactions 2007;7(1):9–16.
[22] Muller R, Koller B, Hilderbrand T, Laib A, Gianolini S, Ruegsegger P. Resolution dependency of microstructural properties of cancellous bone based on three-dimensional mu-tomography. Technology and Health Care 1996;4(1):113–9.
[23] Fouard C, Malandain G. 3-D chamfer distances and norms in anisotropic grids. Image and Vision Computing 2005;23:143–58.
[24] Hojjat S-P, Hardisty MR, Whyne CM. Micro CT based highly-automated 3D segmentation of the rat spine for quantitative analysis of metastatic disease. Journal of Neurosurgery: Spine 2010;13(3):367–70.
[25] Visage Imaging Inc. AmiraDev (Versions 3–5.2) [computer software], http://www.visageimaging.com; 1999–2009.
[26] SPSS Inc. SPSS Comprehensive Statistical Software [computer software], Chicago, IL; 2009.
[27] Tamada T, Sone T, Jo Y, et al. Three-dimensional trabecular bone architecture of the lumbar spine in bone metastasis from prostate cancer: comparison with degenerative sclerosis. Skeletal Radiology 2005;34:149–55.
[28] Peyrin F, Salome M, Cloetens P, Laval-Jeantet AM, Ritman E, Rüegsegger P. Micro-CT examinations of trabecular bone samples at different resolutions: 14, 7 and 2 micron level. Technology and Health Care 1998;6(December (5–6)):391–401.
[29] Niebur GL, Yuen JC, Hsia AC, Keaveny TM. Convergence behavior of high-resolution finite element models of trabecular bone. Journal of Biomechanical Engineering 1999;121(December (6)):629–35.
[30] Bouxsein ML, Boyd SK, Christiansen BA, Guldberg RE, Jepsen KJ, Müller R. Guidelines for assessment of bone microstructure in rodents using micro-computed tomography. Journal of Bone and Mineral Research 2010;25(July (7)):1468–86.

Please cite this article in press as: Hojjat S-P, Whyne CM. Automated quantitative microstructural analysis of metastatically involved vertebrae: Effects of stereologic model and spatial resolution. Med Eng Phys (2010), doi:10.1016/j.medengphy.2010.09.022